



# Fluorometric determination of sulfadiazine by using molecularly imprinted poly(methyl methacrylate) nanobeads doped with manganese(II)-doped ZnS quantum dots

Zhikun Gao<sup>1</sup> · Yu Luan<sup>2</sup> · Yi Lu<sup>3</sup> · Zhiping Zhou<sup>1</sup> · Tianshu Liu<sup>3</sup> · Bolun Li<sup>1</sup> · Zhifeng Qiu<sup>1</sup> · Wenming Yang<sup>1</sup>

Received: 18 March 2019 / Accepted: 31 July 2019 / Published online: 14 August 2019  
© Springer-Verlag GmbH Austria, part of Springer Nature 2019

## Abstract

The surface of poly(methyl methacrylate) nanospheres (PMMA-NSs) was molecularly imprinted with sulfadiazine by a surface imprinting method. Simultaneously, Mn(II)-doped ZnS quantum dots were incorporated into the imprinted PMMA-NSs. The morphology of the fluorescent nanoprobe was characterized by transmission electron microscopy which revealed good spherical core-shell structure and a homogeneous distribution of the QDs. Following binding of sulfadiazine, fluorescence (best measured at excitation/emission maxima of 335/592 nm) is increasingly quenched. The detection range is 5–40  $\mu\text{mol}\cdot\text{L}^{-1}$  of sulfadiazine, and the detection limit is 0.24  $\mu\text{mol}\cdot\text{L}^{-1}$ . The fluorescence quenching mechanism is discussed, and a photo-induced electron transfer process is shown to account for quenching. The fluorescent probe was applied to the determination of sulfadiazine in spiked tap water with recoveries and RSDs of 96.6–100.2% and 2.7–3.9%, respectively. The detection of sulfadiazine in spiked lake water exhibited the recoveries and RSDs with 99.3–104.8% and 1.8–4.2%, respectively.

**Keywords** Molecular imprinting polymers · Sulfadiazine detection · Mn-doped ZnS quantum dots · Absorbability · Quenching mechanism

## Introduction

Sulfadiazine (SD) is commonly used as antibacterial medicine, which is very easy to increase bacterial resistance by releasing a large number of antibiotics into the environment [1]. At present, the high-performance liquid chromatography with tandem mass spectrometry, and high-performance liquid chromatography-electrospray tandem mass spectrometry

sulfonamides are the most common instruments to be used in the detection of the sulfadiazine in wastewater, effluents, surface water and groundwater [2, 3]. Compared with the traditional methods, the emergence of the fluorescent probe method is more easy to realize these advantages such as timely detection, inexpensive raw materials, simple operation, sensitivity and convenience [4].

Semiconductor quantum dots (QDs) are widely used to monitor chemical molecules due to their excellent properties such as tunable absorption, tunable emission spectroscopy and low photobleaching sensitivity [5]. In the past decades, Cadmium QDs are largely researched since the first discovery of Zinc sulfide-capped cadmium selenide QDs [6]. However, the toxicity of cadmium QDs limited their further application in biology labels and detection in the environment [7]. Excitedly, ZnS QDs as an excellent host material have attracted much attention due to its low toxicity, wide direct bandgap and small exciton Bohr radius [8]. Mn-doped ZnS QD causes the red-shift of the initial emission wavelength of ZnS quantum dots from 450 nm to 590 nm [9], where the red-shift was triggered by the variation of transition from  $^4T_1$  to

**Electronic supplementary material** The online version of this article (<https://doi.org/10.1007/s00604-019-3721-1>) contains supplementary material, which is available to authorized users.

✉ Wenming Yang  
ywm@ujs.edu.cn

<sup>1</sup> Institute of Polymer Materials, School of Materials Science and Engineering, Jiangsu University, 301, Xuefu Road, Zhenjiang, Jiangsu Province 212013, China

<sup>2</sup> Zhenjiang Food and Drug Supervision and Inspection Center, Zhenjiang 212004, China

<sup>3</sup> Entry-Exit Inspection Quarantine Bureau, Zhenjiang 212008, China

${}^6\text{A}_1$  in ZnS crystal stimulated by Mn ions [10]. Liu et al. has been reported the Mn-doped ZnS QDs fluorescence probe with high sensitivity, selectivity and fast detecting mercury(II) in tap water [11].

Molecular imprinting polymers (MIPs) has been used to recognize biomolecular, drug molecular and organic molecular because of its special recognition function [12]. Visually, The relationship between MIPs and template molecular is resembled with “lock-key” [13]. Firstly, the template molecular forms a three-dimensional binding under the interaction between templates and monomers via covalent, non-covalent and semi-covalent [14]. Subsequently, a cavity similar to the template formed after the mixture solution polymerized with the addition of cross-linkage [15]. Eventually, these cavities can specifically recognize the target in the complicated liquid again. Xu et al. [16] has reported fluorescence nanobeads for highly sensitive and selective determination of TNT by using a mesoporous structured molecularly imprinted polymers capped carbon dots method.

The large surface area provided by a matrix can enable MIPs with a more stable structure and more cavities [17]. And the stable structure of MIPs warrants the accuracy of special recognition to templates [18]. Thereby, the silica microsphere has been largely utilized as a matrix to support MIPs [19]. However, the MIPs layer is generally difficult imprinted on the surface of silica particles directly due to the smooth surface of silica particles. In most cases, the modification on the surface of silica always is carried out for enhancing the affinity between the MIPs and silica nanobeads. Thereby, the polymer nanosphere as supporting material to attach the MIPs is very advanced because the polymer nanosphere is free-modification owing to its abundant functional groups on its surface. Various polymer microspheres such as polystyrene microsphere, poly(styrene-copolymer) and poly(methyl methacrylate) have been reported by taking different synthetic strategies [20]. Therein, the preparation of poly(methyl methacrylate) nanosphere via the soap-free polymerization method has broadly caused interest due to the non-toxic and simple fabrication [21, 22]. Thereby, a core-shell structure nanobeads based on the PMMA-Ns imprinted with MIPs is synthesized to detect the sulfadiazine. As our best knowledge, the poly(methyl methacrylate) nanosphere (PMMA-Ns) as the matrix to attach MIPs is seldom reported.

## Methods

### Preparation of the core-shell structure fluorescent nanobeads

The MIPs@QDs@PMMA-Ns (MQPs) were synthesized by surface molecular imprinting technology [23], where PMMA-Ns and Mn-doped ZnS QDs were prepared as is given in

Electronic Supporting Material. Firstly, the 10 mL absolute ethanol solution including 125 mg SD, 250  $\mu\text{L}$  3-aminopropyltriethoxysilane (APTES) and 100 mg PMMA-Ns were added into 50 mL flask and stirred for 30 min. Then 1 mL of tetraethoxysilane (TEOS) was added into the above mixture and kept stirring for 10 min. After then, both of 100 mg Mn-doped ZnS QDs and 3.5 ml 6%  $\text{NH}_3\cdot\text{H}_2\text{O}$  were added and continuously stirred for 20 h. The synthesis of NIPs@QDs@PMMANs (NQPs) is similar to MQPs but no SD. The MQPs and NQPs were centrifuged and then washed several times via ethanol and acetic acid (9:1, v/v) to remove the template molecules. Finally, MQPs and NQPs were dried at 50 °C under vacuum.

### Fluorometric analysis of MQPs

The fluorescence analysis was performed on the Lumina fluorescence photometer (USA), where the fluorescence wavelength range of spectra was set from 500 nm to 650 nm under the exciting wavelength was 335 nm. The slit widths and the photomultiplier tube voltage were set at 10 nm and 800 V, respectively. Different concentration SD (from 0 to 40  $\mu\text{mol}\cdot\text{L}^{-1}$ ) was added into 5 mL calibrated test tubes with 2 mL 1  $\text{mg}\cdot\text{mL}^{-1}$  MQPs. Then phosphate buffer (pH = 7.3) was added into tubes until the volume was 5 mL. The fluorescence analysis was carried out after 30 min. Every sample was tested three times.

### The practical sample analysis

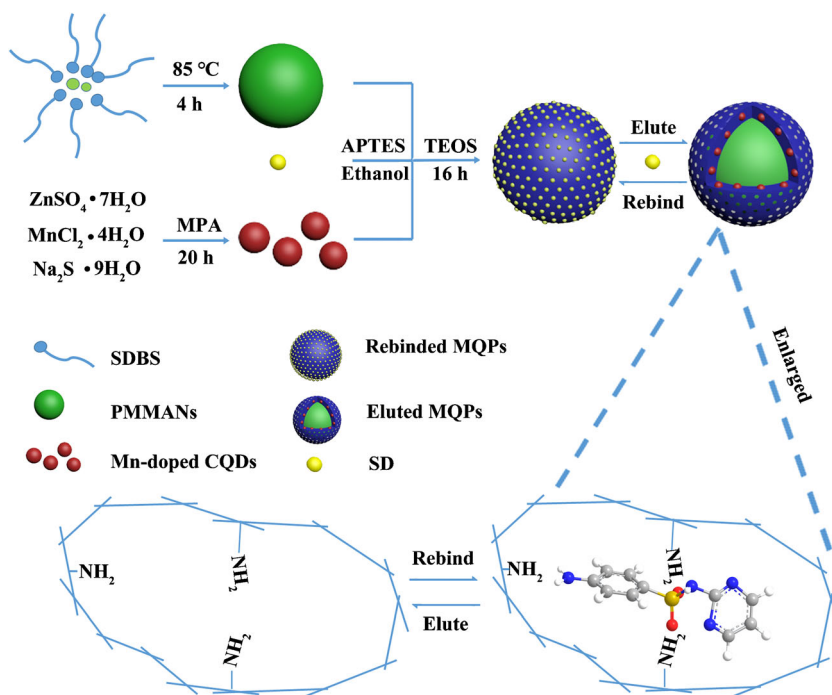
To estimate the practicality, tap water and lake water were selected as a sample to analysis. However, there was no SD found in tap water and lake water. The standard addition recovery method was implemented on analyzing the different prepared SD concentration. The test details as following: firstly, preparing 1  $\text{mmol}\cdot\text{L}^{-1}$  standard SD solution. Secondly, the 2 mL 1  $\text{mg}\cdot\text{mL}^{-1}$  MQPs was added into 5 mL calibrated test tubes. Thirdly, the 1  $\text{mmol}\cdot\text{L}^{-1}$  standard SD solution was diluted into 5.0  $\mu\text{mol}\cdot\text{L}^{-1}$ , 10.0  $\mu\text{mol}\cdot\text{L}^{-1}$  and 15.0  $\mu\text{mol}\cdot\text{L}^{-1}$  based on 5 mL calibrated test tubes via phosphate buffer (pH = 7.3), respectively. Every sample was tested three times.

## Result and discussion

### Preparation of fluorescent nanobeads

Figure 1 systematically describes the process of MQPs preparation. In simple terms, the PMMANs and QDs are prepared using the free-soap method and surface imprinting molecular technology, respectively. And then the Mn-doped ZnS QDs capped with 3-mercaptopropionic acid (MPA) are molecularly imprinted on the surface of PMMANs. In the process of

**Fig. 1** Schematic presentation of PMMA-Ns, Mn-doped ZnS QDs and MQPs, and elution diagram of SD



preparing PMMA-Ns and Mn-doped ZnS QDs, the sodium dodecylbenzene sulfonate and 3-mercaptopropionic acid are used to adjust the diameter of PMMA-Ns and keep the stability of Mn-doped ZnS QDs, respectively. Throughout the process, the PMMANs do not require extra modification due to the abundant ester groups on its surface (Fig.S1). Finally, after the template is eluted from MQPs, the cavities are left and can maximally reabsorb the SD in a complex solution.

### The characterization of the nanobeads

The characteristic of PMMA-Ns, Mn-doped ZnS QDs, MQPs, and NQPs are studied by using TEM, respectively. As is shown in Fig. 2a and b, the PMMANs and Mn-doped ZnS QDs present a good sphere, respectively. Therein, the Mn-doped ZnS QDs possess an excellent mono-dispersity diameter. The average diameter of PMMA-Ns and QDs are around 100 nm and 20 nm, respectively. The patterns of MQPs and NQPs are shown in Fig. 2c and d, respectively. The QDs are observed that it is embedded in the MIPs. As a result, it indicates that the fluorescent nanobeads have a distinct core-shell structure. Additionally, compared with the PMMA-Ns (Fig. 2a), the surface of MQPs is more roughness than the PMMA-Ns. The phenomenon demonstrates that the MIPs are successfully anchored on the surface of PMMA-Ns. The size of MQPs and NQPs is around 100 nm. To further study the QDs location on the surface of PMMA-Ns, the partial enlargement of QDs on the surface of the fluorescence nanobeads is carried out. As is shown in Fig. 2e and f, the QDs are inserted inside of the polymer layer rather than external. However, the diameter of

PMMA-Ns, MQPs, and NQPs are not utterly resembled which may be caused by the nonuniform diameter of PMMA-Ns.

For further ensuring the successful synthesis of MQPs, the FI-IR spectra and XRD pattern are studied, respectively. As is shown in Fig. 3, compared with the Mn-Doped ZnS QDs (curve a), the Mn-doped ZnS QDs capped with MPA (curve b) appear two peaks around 1558.13 cm<sup>-1</sup> and 1401.85 cm<sup>-1</sup>, which are attributed to the asymmetric and symmetric stretching bands of carboxyl, respectively. The result explains that the Mn-doped ZnS QDs have been modified with MPA. However, the characteristic peak of S-H around 2550–2680 cm<sup>-1</sup> is not found, which may be caused by the covalent bonds between thiols and metal atoms of Mn-doped ZnS QDs. The peak of PMMA-Ns (curve c) around 2995.45 cm<sup>-1</sup>, 2954.03 cm<sup>-1</sup>, and 1740.28 cm<sup>-1</sup> are considered as the CH<sub>3</sub> stretching band, the CH<sub>2</sub> of ((-C(R)-(CH<sub>2</sub>)-C(R)-)<sub>n</sub>, n >=4) stretching band and the stretching band of C=O, respectively. The result predicates that the PMMANs is successfully prepared and possess lots of ester groups. The strong and broad peak of MQPs and NQPs (curve d and e) around 1134.67 cm<sup>-1</sup> indicate the Si-O-Si asymmetric band stretching, and the other peaks including 2939.21 cm<sup>-1</sup> and 1545.67 cm<sup>-1</sup> present aliphatic C-H stretching band and N-H band, which demonstrate the presence of the aminopropyl group. The result illustrates the MIPs layer is successfully synthesized and attached to the surface of PMMA-Ns. The XRD analysis is shown in Fig.S2. As a result, the Mn-doped-ZnS QDs have been successfully fabricated, and the MIPs layer also has a protective ability to the Mn-doped ZnS QDs except providing cavities. Also, the result of the XRD study

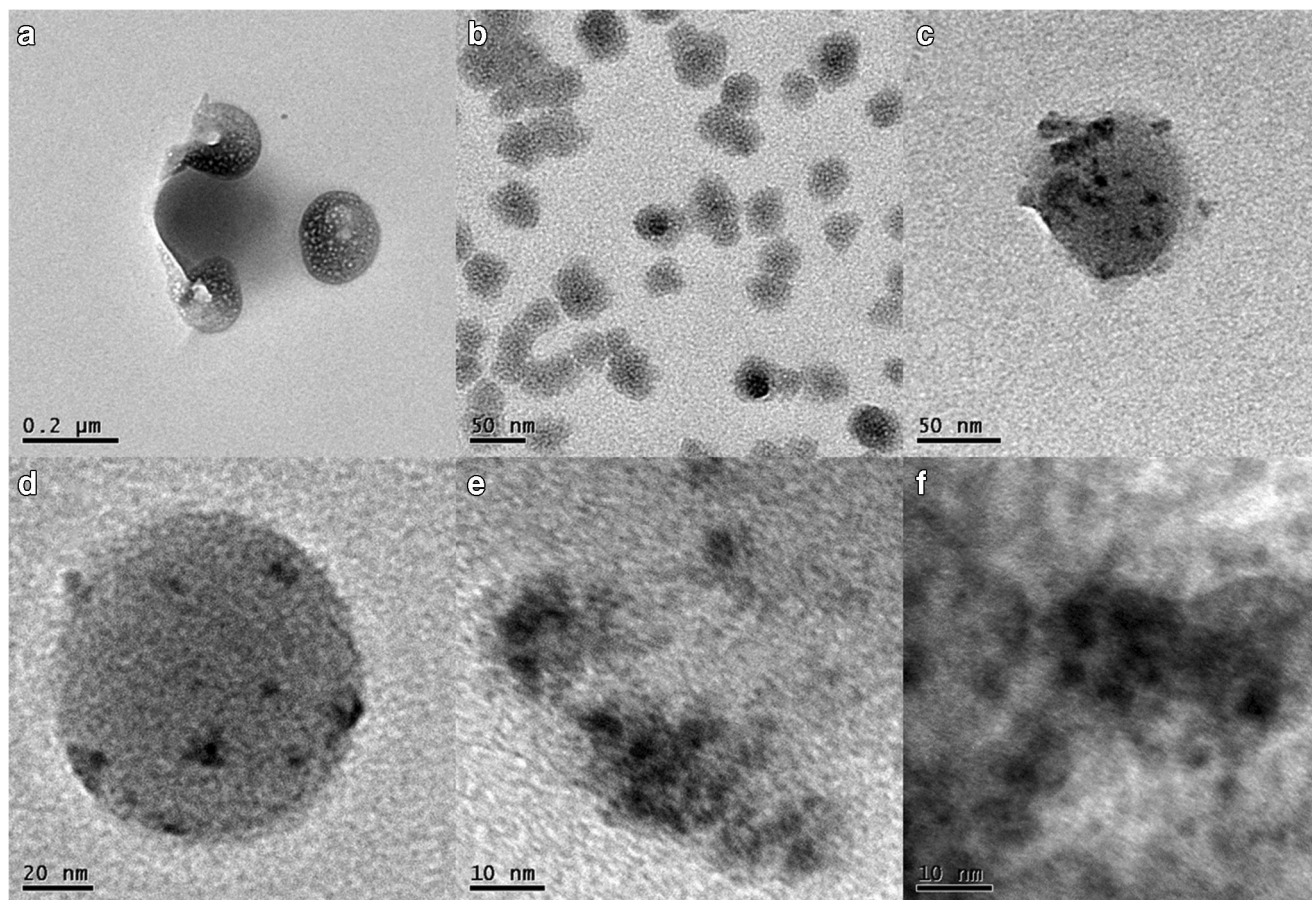


**Fig. 2** The TEM investigation of PMMA-Ns (a), Mn-doped ZnS QDs capped MPA (b), MQPs (c), NQPs (d), enlarged diagram of Mn-doped ZnS QDs on the surface of MQPs (e) and NQPs (f)

further proves that the QDs are embedded inside of MIPs layer. In summary, the core-shell fluorescence nanobeads based on PMMA-Ns are synthesized and imprinted with MIPs layer on the surface of PMMA-Ns.

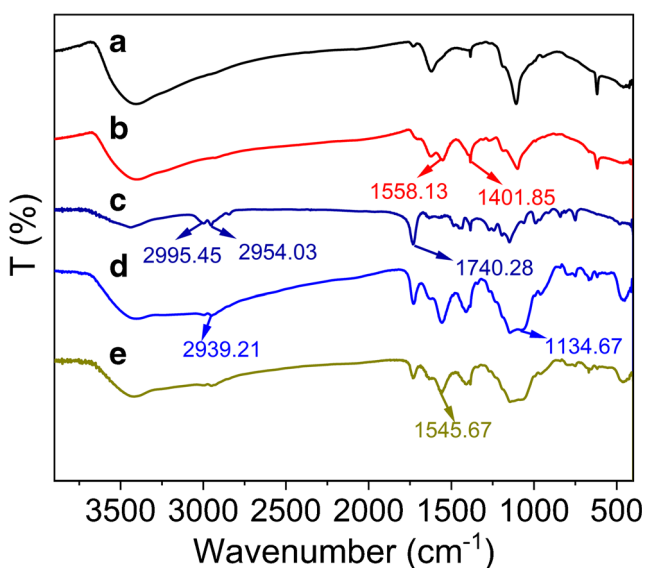


**Fig. 3** The FT-IR research of Mn-doped ZnS QDs (a), Mn-doped ZnS QDs capped MPA (b), PMMA-Ns (c), MQPs (d) and NQPs (e)

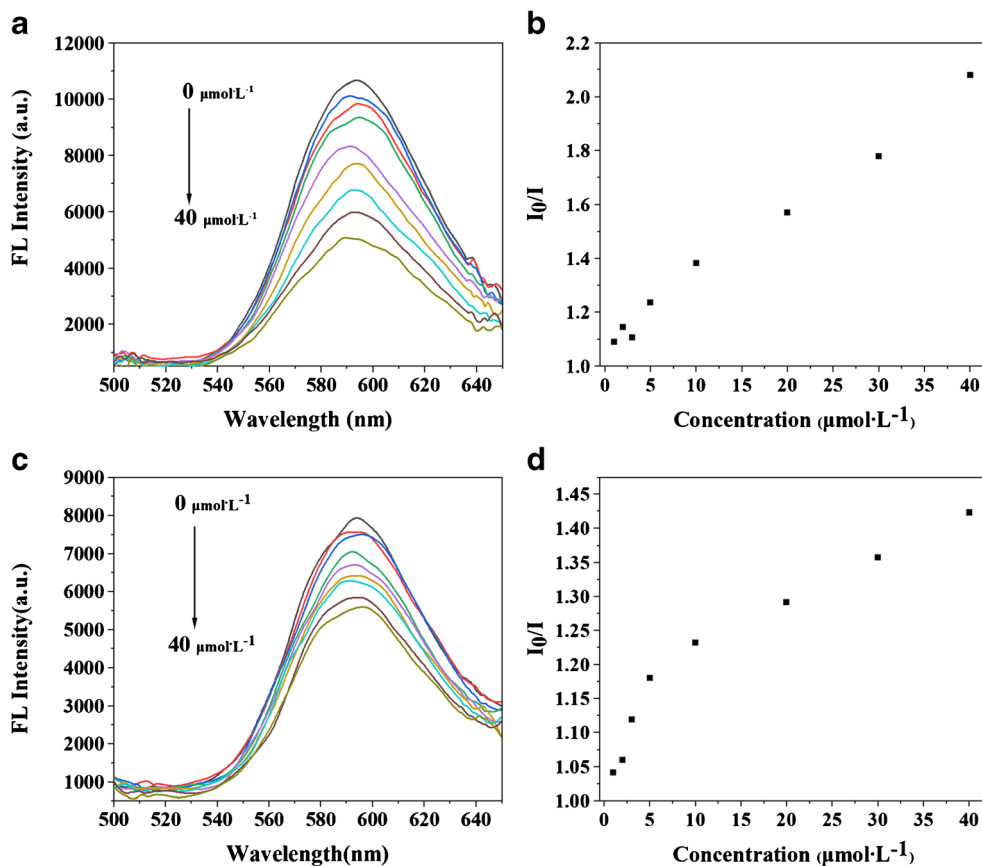
### Fluorescence properties and optimization

The fluorescence intensity result of eluted and un-eluted MQPs and NQPs are investigated and the result shows that the template in MQPs almost is eliminated (Fig.S3). The stability of MQPs fluorescence intensity is investigated and shows that the MQPs can keep stable within 60 min (Fig.S4). The influence of pH value is studied. The data and Figures are given in the Electronic Supporting Material (Fig.S5). As a result, the best pH value is 7.3. All of the following tests are based on the optimized condition.

### Investigation to the concentration of sulfadiazine (SD) and fluorescence intensity of nanobeads

The fluorescent intensity quenching of the MQPs is investigated by adding different concentrations of SD. Under the optimized condition, as is shown in Fig. 4a and c, the fluorescence emission intensity at 592 nm is gradually decreased with increasing concentration from 0 to 40  $\mu\text{mol}\cdot\text{L}^{-1}$ . The result indicates that the MQPs nanobeads can be efficiently quenched by the SD. The  $I_0/I$  study of MQPs and NQPs are shown in Fig. 4b and d, it is very easy found that the MQPs

**Fig. 4** The fluorescence spectra of MQPs (a) and NQPs (c) with increasing concentration of SD from 0 to 40  $\mu\text{mol}\cdot\text{L}^{-1}$  and the  $I_0/I$  variation of MQPs (b) and NQPs (d) with increasing concentration of SD from 0 to 40  $\mu\text{mol}\cdot\text{L}^{-1}$



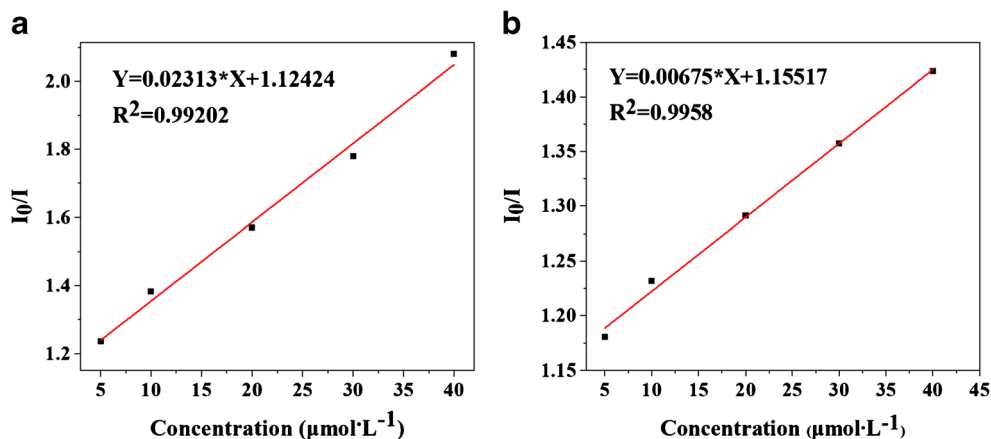
and NQPs have linear correlation within 5 to 40  $\mu\text{mol}\cdot\text{L}^{-1}$  SD. The fitted curve of MQPs and NQPs within the linear correlation range are shown in Fig. 5a and b, respectively. The linear correlation fitted curve of MQPs and NQPs are described as following traditional Stern-Volmer equation, respectively:

$$Y_1 = 0.02313 \cdot X + 1.12424 \quad (R_1^2 = 0.9920) \quad (1)$$

$$Y_2 = 0.00675 \cdot X + 1.15517 \quad (R_2^2 = 0.9958) \quad (2)$$

Where  $Y_1$  and  $Y_2$  are the  $I_0 / I$  of MQPs and NQPs, respectively. The  $I_0$  and  $I$  are the fluorescence intensity in the absence and presence of SD, respectively.  $X$  is the concentration of SD. The Stern-Volmer constant of MQPs and NQPs are 0.02313 and 0.00675, respectively. The correlation coefficient of MQPs and NQPs is 0.99202 and 0.9958, respectively. The  $3\sigma / S$  is utilized to calculate the detection limit of MQPs, where the  $\sigma$  is the standard deviation of the blank signal and  $S$  is the slope of the Stern-Volmer equation. As a result, the detection limit is 0.24  $\mu\text{mol}\cdot\text{L}^{-1}$ . The low detection limit may be attributed to the PMMA nanosphere that provides a large

**Fig. 5** The linear fitted curve of MQPs (a) and NQPs (b) in the range of SD concentration from 5 to 40  $\mu\text{mol}\cdot\text{L}^{-1}$



surface area and stable structure for MIPs. Also, the quenching extent of NQPs is less than MQPs, which is due to no imprinting cavities on the surface of NQPs. The IF ( $K_{sv\_MIP} / K_{sv\_NIP}$ ) is calculated into 3.43, which indicates the MQPs have an excellent absorbability to SD. In conclusion, the proposed MQPs can be efficiently quenched by SD. Both of MQPs and NQPs have a good linear correlation within the SD concentration range from 5 to 40  $\mu\text{mol}\cdot\text{L}^{-1}$ . The limit of detection of MQPs is 0.24  $\mu\text{mol}\cdot\text{L}^{-1}$ . A review of the reported methods for the detection of SD is investigated. As is shown in Table S1, the results show that LOD of MQPs is close to reported methods, which may be owing to the PMMA-Ns providing a good surface area.

### The absorbability of the nanobeads to sulfadiazine (SD)

The absorbability of MQPs is investigated by utilizing three similar molecules SM, SM2, and SMZ, respectively (Fig.S6). As is shown in Fig. 6, compared with other similar molecules, the I<sub>0</sub>/I of MQPs is largest in the existence of SD. The result illustrates that the MQPs have a maximal absorbability to SD, which is attributed to the large quantities of imprinting cavities on the surface of MQPs. Simultaneously, the I<sub>0</sub>/I variation of NQPs in the presence of SD, SM and SMZ are also studied. It finds that the quenching extent of SD and other similar molecules to NQPs is very lower than MQPs. The lower quenching extent is due to no imprinting cavities on the surface of NQPs. However, a similar molecular still influences the fluorescence intensity of MQPs. Thereby, the uncertainty method is used to further studying the absorbability of MQPs to SD. The Figures and graph are given in Electronic Supporting Material (Fig.S7). As a result, the proposed MQPs has a good special absorption capacity in the mixture solution. Also, the influence of high concentration similar

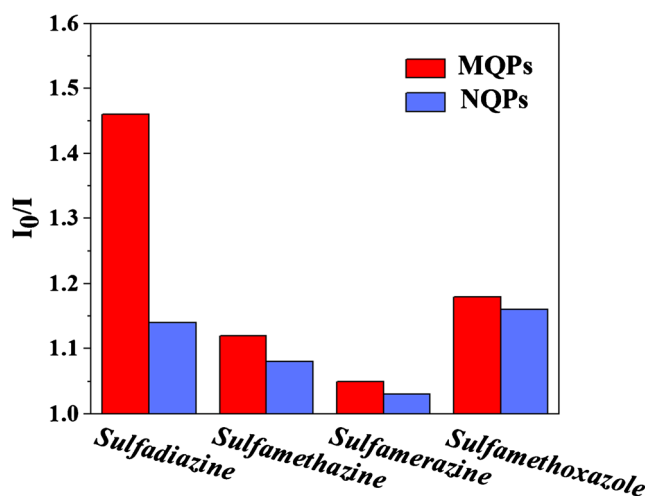


**Fig. 6** The absorbability research of MQPs and NQPs to 20  $\mu\text{mol}\cdot\text{L}^{-1}$  SD and  $\mu\text{mol}\cdot\text{L}^{-1}$  similar molecules including SM, SM<sub>2</sub> and SMZ

molecules to the accuracy of monitoring SD is investigated and shown in Fig.S8. As a result, the accuracy of detection to low concentration SD in complex solution with high concentration similar molecules does not have the desired effect.

### Practical application to analyze tap water and lake water

The practical application of fluorescence nanobeads is studied using tap water and lake water samples. As is shown in Table 1, no SD is found from three tap water samples. Thereby, the practical application is carried out by using the standard addition recovery method. Three different concentration solutions of SD are prepared with the addition of SD, which are 5.0  $\mu\text{mol}\cdot\text{L}^{-1}$ , 10.0  $\mu\text{mol}\cdot\text{L}^{-1}$ , and 15.0  $\mu\text{mol}\cdot\text{L}^{-1}$ , respectively. After analysis the three prepared concentration solutions of SD by MQPs, the result shows that the quantitative recoveries in tap water ranged from 96.6% to 100.2%, and the relative standard deviation (RSD) ranged from 2.7% to 3.9%. Similarly, no SD is not found in lake water also. The same method is used to analyze the SD in lake water by using proposed nanobeads. The result shows that the quantitative recoveries rate in lake water ranges from 99.3% to 104.8%, and RSD in lake water ranges from 1.8% to 4.2%. Both tap water and lake water results indicate that the MQPs possess the potential applicability to detect SD in real water. Also, the recovery range and relative standard deviation investigation on reported similar methods are listed in Table S2. After comparing with other reported methods, the result shows that the proposed MQPs have the same or more excellent practical application in real water.

**Table 1** The practical application of MQPs with the different concentration SD (0  $\mu\text{mol}\cdot\text{L}^{-1}$ , 5  $\mu\text{mol}\cdot\text{L}^{-1}$ , 10  $\mu\text{mol}\cdot\text{L}^{-1}$  and 15  $\mu\text{mol}\cdot\text{L}^{-1}$ ) in tap water and lake water ( $n = 3$ )

Sample	Concentration of SD ( $\mu\text{M}$ )		Recovery (%)	RSD (%)
	Add	Found		
Tap water 1	0	No found	0	0
	5	4.83	96.6	3.2
Tap water 2	0	No found	0	0
	10	9.97	99.7	2.7
Tap water 3	0	No found	0	0
	15	15.03	100.2	3.9
Lake water 1	0	No found	0	0
	5	5.24	104.8	4.2
Lake water 2	0	No found	0	0
	10	9.96	99.6	2.3
Lake water 3	0	No found	0	0
	15	14.89	99.3	1.8

## Quenching mechanism

The fluorescent quenching mechanism is discussed. At present, the popular FL quenching mechanisms are divided into two mechanisms including photoinduced electronic transfer (PET) and the Forster resonance energy transfer (FRET). The FRET quenching mechanism requires the overlap between the emission spectrum of electron donor and the absorbed spectrum of electron acceptor. However, the fluorescence of SD is not found in the experiment (date is not given). As is shown in Fig.S9, the UV absorption wavelength of SD (a) and the emission wavelength of MQPs (b) have no overlap. Therefore, the quenching mechanism may be not FRET. After compared with the UV-vis absorbance of SD, MQPs, and mixture of SD and MQPs, as is shown in Fig.S10, the MQPs does not exist the absorptive peaks, and the SD has two absorptive peaks around 240 nm and 256 nm, respectively. After adding the SD into MQPs, the two peaks have a little change and located at 241 nm and 255 nm. The result indicates that the SD may react with the MPA on the surface of MQPs, which results the electrons transfer from excited MQPs to SD. Also, the SD has many strong electronegativity elements in its structure (shown in Fig.S6, sulfadiazine) such as nitrogen, oxygen, and sulfur, which make SD be very easy to absorb a charge from excited MQPs, and therefore the fluorescence intensity of MQPs decrease. In conclusion, the PET may be suggested as a possible fluorescent quenching mechanism.

## Conclusion

The core-shell fluorescent nanobeads based on PMMA-Ns are successfully synthesized and applied to the detection of SD. The lower LOD allows core-shell structured fluorescent nanobeads to have potential applications for fast and easy monitoring SD in real water. In addition, polymer nanobeads as a MIPs-supporting matrix can provide other researchers with new ways to further study polymer-based core-shell nanospheres. However, the detection accuracy of MQPs to low-concentration SD in high-concentration similar molecules still needs further improvement. Making full use of the abundant functional groups on the polymer nanoparticles may realize the accurate detection of contaminants in complex systems.

**Acknowledgements** This work was financially supported by the National Natural Science Foundation of China (Grant No. 21677064), Zhenjiang Natural Science Foundation of China (Grant Nos. SH2017046, SH2017048 and SH2017055), Scientific Research Foundation of Jiangsu University (Grant No. 17A008).

**Compliance with ethical standards** The author(s) declare that they have no competing interests.

## References

- Biošić M, Mitrevski M, Babić S (2017) Environmental behavior of sulfadiazine, sulfamethazine, and their metabolites. *Environ Sci Pollut Res Int* 24:9802–9812
- Silvia Diaz-Cruz M, Jesus Garcia-Galan M, Barcelo D (2008) Highly sensitive simultaneous determination of sulfonamide antibiotics and one metabolite in environmental waters by liquid chromatography-quadrupole linear ion trap-mass spectrometry. *J Chromatogr A* 1193:50–59
- Perisa M, Babić S (2014) Simultaneous determination of pharmaceuticals and some of their metabolites in wastewaters by high performance liquid chromatography with tandem mass spectrometry. *J Sep Sci* 37:1289–1296
- Zhao T, Hou XD, Xie YN, Wu L, Wu P (2013) Phosphorescent sensing of Cr<sup>3+</sup> with protein-functionalized Mn-doped ZnS quantum dots. *Analyst* 138:6589–6594
- Zhang JR, Huang WT, Xie WY, Wen T, Luo HQ, Li NB (2012) Highly sensitive, selective, and rapid fluorescence Hg<sup>2+</sup> sensor based on DNA duplexes of poly(dT) and graphene oxide. *Analyst* 137:3300–3305
- Chan WC, Nie S (1998) Quantum dot bioconjugates for ultrasensitive nonisotopic detection. *Science* 281:2016–2018
- Pradhan N, Goorskey D, Thessing J, Peng XG (2005) An alternative of CdSe nanocrystal emitters: pure and tunable impurity emissions in ZnSe nanocrystals. *J Am Chem Soc* 127:17586–17587
- Labiadh H, Sellami B, Khazri A, Saidani W, Khemais S (2017) Optical properties and toxicity of undoped and Mn-doped ZnS semiconductor nanoparticles synthesized through the aqueous route. *Opt Mater* 64:179–186
- Suyver JF, Wuister SF, Kelly JJ, Meijerink A (2001) Synthesis and photoluminescence of nanocrystalline ZnS : Mn<sup>2+</sup>. *Nano Lett* 1: 429–433
- Bol AA, Meijerink A (1998) Long-lived Mn<sup>2+</sup> emission in nanocrystalline ZnS:Mn<sup>2+</sup>. *Phys Rev B* 58:R15997–R16000
- Liu X, Zhan XS, Wu FY, Ma LH (2015) Mn(II)-doped ZnS quantum dots modified with Tiopronin for mercury(II) detection. *Aust J Chem* 68:315–321
- Zarejousheghani M, Fiedler P, Moder M, Borsdorf H (2014) Selective mixed-bed solid phase extraction of atrazine herbicide from environmental water samples using molecularly imprinted polymer. *Talanta* 129:132–138
- Yu YJ, Zhang Q, Buscaglia J, Chang CC, Liu Y, Yang ZH, Guo YC, Wang YT, Levon K, Rafailovich M (2016) Quantitative real-time detection of carcinoembryonic antigen (CEA) from pancreatic cyst fluid using 3-D surface molecular imprinting. *Analyst* 141:4424–4431
- Huang DL, Wang RZ, Liu YG, Zeng GM, Lai C, Xu P, Lu BA, Xu JJ, Wang C, Huang C (2015) Application of molecularly imprinted polymers in wastewater treatment: a review. *Environ Sci Pollut Res Int* 22:963–977
- Zaidi SA (2018) Development of molecular imprinted polymers based strategies for the determination of dopamine. *Sensors Actuators B Chem* 265:488–497
- Xu SF, Lu HZ (2016) Mesoporous structured MIPs@CDs fluorescence sensor for highly sensitive detection of TNT. *Biosens Bioelectron* 85:950–956
- Lofgreen JE, Ozin GA (2014) Controlling morphology and porosity to improve performance of molecularly imprinted sol-gel silica. *Chem Soc Rev* 43:911–933
- Huynh TP, Kutner W (2015) Molecularly imprinted polymers as recognition materials for electronic tongues. *Biosens Bioelectron* 74:856–864
- Zhou ZP, Li T, Xu WZ, Huang WH, Wang NW, Yang WM (2017) Synthesis and characterization of fluorescence molecularly

- imprinted polymers as sensor for highly sensitive detection of dibutyl phthalate from tap water samples. *Sensors Actuators B Chem* 240:1114–1122
20. Yan R, Zhang YY, Wang XH, Xu JX, Wang D, Zhang WQ (2012) Synthesis of porous poly(styrene-co-acrylic acid) microspheres through one-step soap-free emulsion polymerization: whys and wherefores. *J Colloid Interface Sci* 368:220–225
  21. Zhu AP, Shi ZH, Cai AY, Zhao F, Liao TQ (2008) Synthesis of core-shell PMMA-SiO<sub>2</sub> nanoparticles with suspension-dispersion-polymerization in an aqueous system and its effect on mechanical properties of PVC composites. *Polym Test* 27:540–547
  22. Whitby GS, Gross MD, Miller JR, Costanza AJ (1955) Emulsifier-free polymerization in aqueous media. *J Polym Sci* 16:549–576
  23. Wang HF, He Y, Ji TR, Yan XP (2009) Surface molecular imprinting on Mn-doped ZnS quantum dots for room-temperature phosphorescence Optosensing of pentachlorophenol in water. *Anal Chem* 81:1615–1621

**Publisher's note** Springer Nature remains neutral with regard to jurisdictional claims in published maps and institutional affiliations.